Conducting Carbon Wires in Ordered, Nanometer-Sized Channels

Chun-Guey Wu and Thomas Bein*

The encapsulation of graphite-type carbon wires in the regular, 3-nanometer-wide hexagonal channels of the mesoporous host MCM-41 is reported. Acrylonitrile monomers are introduced through vapor or solution transfer and polymerized in the channels with external radical initiators. Pyrolysis of the intrachannel polyacrylonitrile results in filaments whose microwave conductivity is about 10 times that of bulk carbonized polyacrylonitrile. The MCM host plays a key role in ordering the carbon structure, most likely through the parallel alignment of the precursor polymer chains in the channels. The fabrication of stable carbon filaments in ordered, nanometer-sized channels represents an important step toward the development of nanometer electronics.

Intensive efforts under way to increase computing speed and storage density in information processing could culminate in the design of nanometer-sized, molecule-based electronic devices (1). One major challenge in this context is to achieve communication with individual nanometer-sized structures or molecules. Encapsulation of conducting structures in ordered, insulating host systems is a promising approach toward controlled electronic access to individual nanometer-sized objects.

We have used the well-defined subnanometer-sized channels of zeolites as hosts for several different conjugated polymers such as polypyrrole, but the small diameter of these channels appears to inhibit significant conductivity (2, 3). Conducting polymers have also been prepared in the much larger, random pores (approximately 0.1 to 1 μm) of insulating host membranes (4). Our recent study of polyaniline in MCM-41 demonstrates conductivity at the nanometer level (5). Graphitic carbon is attractive for the design of conducting nanostructures because of its inherent stability and high conductivity. Efforts aimed at controlling the structure of randomly grown carbon nanotubes are under way (6). We have now succeeded in encapsulating conducting carbon "wires" in the regular, 3-nm-wide hexagonal channels of the mesoporous aluminosilicate host MCM-41 (7, 8). The MCM host plays a key role in ordering the carbon structure, leading to enhanced conductivity compared with that possible in the corresponding bulk material.

The carbon wires in MCM channels are based on pyrolyzed (9) encapsulated polyacrylonitrile (PAN); polymerization of acrylonitrile is known to proceed rapidly and exothermically in the presence of free radicals or anionic initiators (10). The pyrolysis of PAN

leads initially to the formation of a ladder polymer by cyclization through the nitrile pendant group (11), followed by graphitization and increasing electronic conductivity at higher temperatures (12, 13). The MCM-41 host for the encapsulation experiments was synthesized with $C_{16}H_{33}N(CH_3)_3OH$ according to the method given in (7), calcined at 580°C in air, and evacuated at 400°C and 10^{-5} torr. The host was contacted with degassed acrylonitrile vapor at room temperature for 4 hours and then briefly evacuated, resulting in a typical uptake of 0.54 g of acrylonitrile per gram of host (sample AC-MCM) (Fig. 1). This loading corresponds well with the saturation expected from the pore volume (0.64 ml/g), obtained from nitrogen absorption isotherms.

For polymerization, sample AC-MCM was mixed with distilled water under nitrogen (typically 1.00 g with 20 ml of water). The temperature was raised to 40°C, and then 20 mg of $K_2S_2O_8$ and 10 mg of $NaHSO_3$ were added as radical initiators. The mixture was stirred for 20 hours at 40°C, and the resulting white solid (PAN-MCM) was washed with water and then evacuated.

The polymer in MCM shows a solid-state nuclear magnetic resonance signature similar to that of bulk PAN [=CH– and =CH_2 groups at ~30 parts per million (ppm) and –CN groups at 123 ppm] (3, 14). The polymer chain length of extracted material, obtained from gel permeation chromatography (in N,N-dimethyl formamide at 50°C, PAN standard), is on the order of 1000 monomers (peak molecular weight 60,000 in a monomodal distribution, compared with 120,000 for the bulk material made under similar conditions). The encapsulated chains are long enough to span significant parts of the MCM-41 crystals (about 250 nm) but shorter than in bulk PAN, which may reflect diffusional limitations or channel defects in the host channels.

Thermal treatment of PAN-MCM in nitrogen flow between 350° and 1000°C for 24 hours led to color changes from white to black, with a concomitant weight loss. The polymer content stabilized at ~10% (by weight) between 800° and 1000°C. The N/C ratio of PAN-MCM also dropped during heating, from 0.32 at room temperature to 0.07 at 1000°C. Similar compositional changes reflecting the graphitization process were also observed in bulk and thin-film experiments (10). The x-ray crystallinity of the host remained intact even after pyrolysis at 1000°C. Transmission electron micrographs of pyrolyzed PAN-MCM showed clean faces of the mesoporous host crystals when viewed both along and normal to the channel directions. Therefore, any significant buildup of external carbon phases and associated pore blockage can be excluded. Nitrogen sorption experiments showed reduced pore volumes for the PAN-loaded MCM host and for the pyrolyzed samples, demonstrating the formation of PAN and graphite-like material inside the host channels.

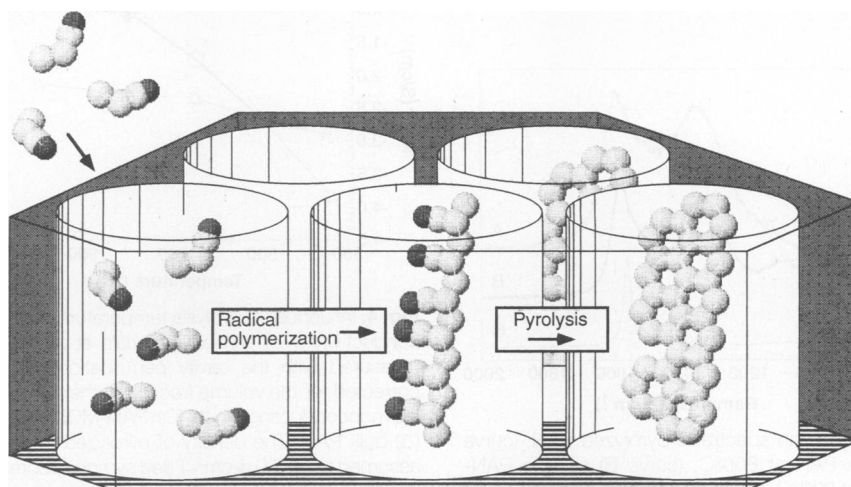Raman scattering has been identified as a

Department of Chemistry, Purdue University, West Lafayette, IN 47907, USA.

*To whom correspondence should be addressed.

Fig. 1. Schematic representation of the formation of carbon wires in the MCM-41 channel host.

sensitive probe for the structure of carbon materials (*15*, *16*). The micro-Raman spectra of pyrolyzed PAN-MCM show two distinct peaks, the Raman-allowed E_{2g} graphitic peak at ~1580 cm^{-1} (G) and the D band at ~1360 cm^{-1} that is associated with small domain sizes (Fig. 2). The integrated relative intensities of the D mode versus the graphitic G mode, $I(D/G)$, are consistently smaller in the pyrolyzed PAN-MCM samples than in the corresponding bulk materials. For example, after pyrolysis at 800°C, $I = 1.52$ for PAN-MCM and 1.85 for the bulk material. We used the reported empirical correlation between these ratios and graphitic domain sizes (*16*) and found that the ordered domains in pyrolyzed PAN-MCM extend ~30 Å versus 24 Å in the bulk material.

Thin-film studies of pyrolyzed PAN (preheated in air at 220°C) confirmed that treatments up to 1200°C produce only very small graphitic domains (<20 Å) (*13*). The linewidth of the G mode relates to disorder within the carbon sheets (*16*). In PAN-MCM (800°C), the linewidth is 100 cm^{-1}, whereas in the bulk material, it is 130 cm^{-1}. The above data show that the MCM host plays a key role in ordering the growing graphitic sheets, most likely through the parallel alignment of the precursor polymer chains in the channels.

The properties of the charge carriers on these carbon wires are of particular interest. When a sample of PAN-MCM was heated to 350°C and higher, a single electron spin resonance (ESR) line of increasing intensity was observed (*g* factor of 2.0028), similar to previous observations with PAN fibers (*17*). The linewidth in PAN-MCM dropped from 6 to ~3 G between 350° and 500°C and remained fairly constant at higher pyrolysis temperatures. In contrast, the bulk material shows a continuous decrease in linewidth and reaches a final value of 0.33 G at 1000°C (Fig. 3). The greater ESR linewidth of pyrolyzed PAN in the MCM host is prob-
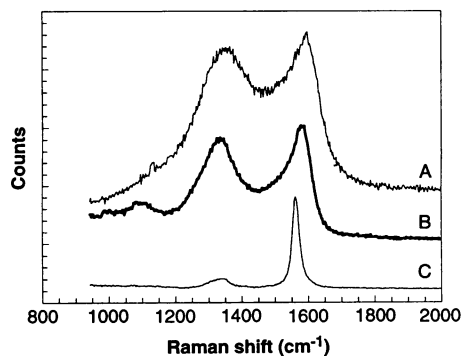
ably the result of dipolar interactions of the carbon material with the channel walls.

Conductivity studies of bulk pyrolyzed PAN have shown that metallic conduction pathways and localized spins coexist (*17*). We then considered how the carbon material behaves when it is encapsulated in nanometer-sized channels. We measured the dc conductivity of pressed pellets of the composites at room temperature. The dc conductivity of PAN-MCM for all pyrolysis temperatures up to 800°C is in the range of 10^{-7} S/cm, similar to the conductivity of unloaded MCM host under ambient conditions and many orders of magnitude lower than that for bulk PAN. This result confirms that the carbon material is located inside the insulating MCM channels and that no percolating conducting paths develop on the external crystal surfaces. The contactless microwave cavity perturbation technique (*18*) at 2.63 GHz (measuring changes in the quality factor Q of an 8 mm by 110 mm by 200 mm rectangular cavity) was used to probe the charge transport in the encapsulated carbon wires. The micro-
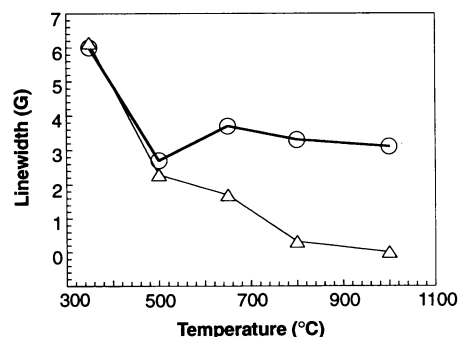

Fig. 3. Effect of pyrolysis temperature on the ESR linewidth at $g = 2.0028$: (O) PAN-MCM adduct; (△) bulk PAN.
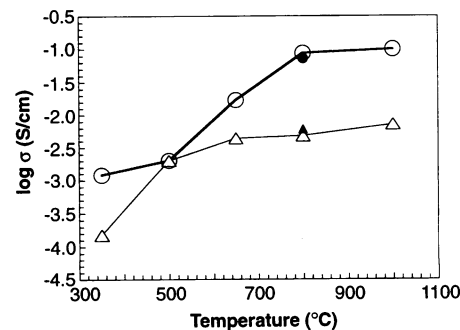

Fig. 4. Influence of pyrolysis temperature on the ac conductivity σ of carbon materials at 2.63 GHz, measured with the cavity perturbation method, corrected for the volume fraction of the polymer in the nonconducting host: (O) PAN-MCM adduct; (△) bulk PAN. The density of pyrolyzed PAN was assumed to be 2.0 g/cm^3. Filled symbols represent samples treated in air at 225°C for 6 hours before pyrolysis under nitrogen.

wave conductivity of dry PAN-MCM was found to increase with pyrolysis temperature and was about 10 times that of bulk PAN pyrolyzed under the same conditions, reaching 10^{-1} S/cm at 1000°C (Fig. 4). Pretreatment of PAN-MCM in air at 225°C leads to a similar carbon content, ac conductivities, and Raman spectra. We explain this striking result as being caused by the different order of the graphitic material in the two environments: As determined in the Raman study, the MCM channels assist in the formation of larger domains of ordered graphite, which result in higher conductivity.

This significant low-field conductivity of PAN-MCM demonstrates that carbon wires can be encapsulated in nanometer-sized channels and still support mobile charge carriers. We have established that oxidized polypyrrole chains in the channels of zeolite Y and mordenite (0.7-nm channels) do not exhibit significant ac conductivity up to 1 GHz, suggesting trapped charge carriers and a lack of interchain contacts (*19*). In contrast, the channels in the MCM host provide more space, allowing some important transverse delocalization in the graphitic structure. The fabrication of these types of stabilized conducting systems (wires based on carbon in nanometer-sized channels) will be important for the understanding of charge transport at the nanometer scale and for the development of nanometer-sized electronic devices.

REFERENCES AND NOTES

1. C. Carter, *Molecular Electronic Devices* (Dekker, New York, 1982); A. Farazdel, M. Dupuis, E. Clementi, A. Arivam, *J. Am. Chem. Soc.* **112**, 4206 (1990); J. M. Tour, R. Wu, J. S. Schumm, *ibid.*, p. 5662; N. S. Hush, A. T. Wong, G. B. Bacskay, J. R. Reimers, *ibid.*, p. 4192; J. M. Lehn, *Angew. Chem. Int. Ed. Engl.* **29**, 1304 (1990); J. J. Hopfield, J. N. Onuchic, B. N. Beratan, *J. Phys. Chem.* **93**, 6350 (1989).
2. T. Bein and P. Enzel, *Angew. Chem. Int. Ed. Engl.* **28**, 1692 (1989); P. Enzel and T. Bein, *J. Phys. Chem.* **93**, 6270 (1989); *J. Chem. Soc. Chem. Commun.* **1989**, 1326 (1989).
3. P. Enzel and T. Bein, *Chem. Mater.* **4**, 819 (1992).
4. C. R. Martin, R. Parthasarathy, V. Menon, *Synth. Met.* **55–57**, 1165 (1993), and references therein.
5. C.-G. Wu and T. Bein, *Science* **264**, 1757 (1994).
6. R. F. Ruoff, J. Tersoff, D. C. Lorents, S. Subramoney, B. Chan, *Nature* **364**, 514 (1993); Y. Wang, *J. Am. Chem. Soc.* **116**, 397 (1994).
7. J. S. Beck *et al.*, *J. Am. Chem. Soc.* **114**, 10834 (1992).
8. A. Monnier *et al.*, *Science* **261**, 1299 (1993).
9. J. E. Bailey and A. J. Clarke, *Nature* **234**, 529 (1971); L. H. Peebles, P. Peyser, A. W. Snow, W. C. Peeters, *Carbon* **28**, 707 (1990).
10. H. F. Mark *et al.* (Editorial Board), *Encyclopedia of Polymer Science and Engineering* (Wiley, New York, 1985), vol. 1, p. 426.
11. W. T. K. Stevenson, A. Garton, J. A. Ripmeester, D. M. Wiles, *Polym. Degradation Stab.* **15**, 125 (1986).
12. P. J. Goodhew, A. J. Clarke, J. E. Bailey, *Mater. Sci. Eng.* **17**, 3 (1975).
13. C. L. Renschler, A. P. Sylwester, L. V. Salgado, *J. Mater. Res.* **4**, 452 (1989).
14. J. C. Randall, C. J. Ruff, M. Kelchtermans, B. H. Gregory, *Macromolecules* **25**, 2624 (1992).
15. A. M. Rao, A. W. P. Fung, M. S. Dresselhaus, M.

Fig. 2. Raman spectra of pyrolyzed PAN: (curve A) bulk PAN at 800°C, (curve B) sample PAN-MCM at 800°C, (curve C) graphite. Excitation was with ~10 mW at 514.5 nm.

Endo, *J. Mater. Res.* **7**, 1788 (1992).
16. D. S. Knight and W. B. White, *ibid.* **4**, 385 (1989).
17. N. R. Lerner, *J. Appl. Phys.* **52**, 6757 (1981).
18. D. C. Dube, M. T. Lanagan, J. H. Kim, S. J. Jang, *ibid.* **63**, 2466 (1988).
19. L. Zuppiroli, F. Beuneu, J. Mory, P. Enzel, T. Bein,

Synth. Met. **55–57**, 5081 (1993).
20. This research was supported in part by the Sprague Electric Company. We thank S. Esnouf for contributions to the ac conductivity measurements.

Precipitation Hardening in the First Aerospace Aluminum Alloy: The Wright *Flyer* Crankcase

Frank W. Gayle and Martha Goodway

Aluminum has had an essential part in aerospace history from its very inception: An aluminum copper alloy (with a copper composition of 8 percent by weight) was used in the engine that powered the historic first flight of the Wright brothers in 1903. Examination of this alloy shows that it is precipitation-hardened by Guinier-Preston zones in a bimodal distribution, with larger zones (10 to 22 nanometers) originating in the casting practice and finer ones (3 nanometers) resulting from ambient aging over the last 90 years. The precipitation hardening in the Wright *Flyer* crankcase occurred earlier than the experiments of Wilm in 1909, when such hardening was first discovered, and predates the accepted first aerospace application of precipitation-hardened aluminum in 1910.

Progress in the aerospace industry, from the development of commercial airliners to the space shuttle, has been dependent on the great strength and fracture toughness provided by precipitation hardening (1), especially in aluminum-based alloys. In the historic first flight of 17 December 1903, Wilbur and Orville Wright used an Al–8% copper alloy (with about 1.0% iron and 0.4% silicon as impurities) (2) for the crankcase of their self-designed internal combustion engine because of the alloy's strength and the weight requirements of the aircraft. This alloy represented the state of the art in casting alloys at the turn of the century, primarily because of its good casting qualities (3). The crankcase of the original engine has recently been identified (4, 5); because it was the only Al part on the Wright *Flyer*, it thus became the first aerospace Al. Our study here reports the microstructure and strengthening mechanisms operating in this crankcase alloy.

Small samples of the *Flyer* crankcase were taken from three locations in the crankcase wall (6), which was approximately 4 to 5 mm thick. The microstructure (Fig. 1) consists of a typical solidification structure of α-Al dendrites (7) [face-centered-cubic (fcc) crystal structure] with interdendritic blocky θ-Al₂Cu and needlelike ω-Al₇Cu₂Fe phases. Dendrite arm spacings ranged from 40 to 80 μm, which suggests that the local solidification time was approximately 2 min (8). A gradient of Cu

content across the dendrites, or coring, is expected in Al-Cu solidification structures and was analyzed by electron microprobe (9). The concentration of Cu was about 2.25% near the dendrite centers and approximately 4.75% near the surface of the dendrites (10). Most of the Cu in the alloy is thus present in the interdendritic intermetallic phases Al_2Cu and Al_7Cu_2Fe.

A higher spatial resolution than that attainable with optical microscopy is required to detect precipitates formed in the solid state in Al alloys. Transmission electron microscopy (TEM) (Fig. 2) revealed a remark-
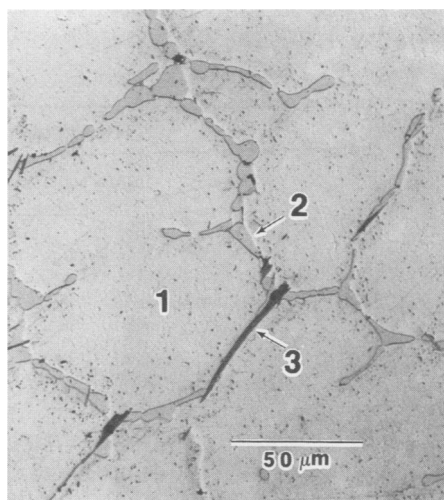

Fig. 1. Typical microstructure of the Wright *Flyer* crankcase (light optical micrograph), showing dendrites (area 1) of fcc Al(Cu) and the interdendritic second phases Al_2Cu (arrow 2) and Al_7Cu_2Fe (arrow 3). The dendrites exhibit coring wherein the center of each dendrite is approximately 2.25% Cu, increasing to 4.75% Cu at the edge of the dendrite.

ably well developed Guinier-Preston (GP) zone structure (1, 11, 12). These metastable GP zones consist of disks of Cu, a single atomic layer in thickness, lying on the three equivalent {100} planes within the fcc Al matrix. GP zones are readily imaged in TEM because of the large strain field associated with the zone, resulting in images several atomic layers in apparent thickness. Two mutually perpendicular variants, viewed edge-on, are apparent in this specimen orientation, viewed down a cube orientation of the matrix, or **B** = [001]. The zones are predominantly 10 to 20 nm in diameter. An occasional precipitate of θ'-Al₂Cu with a neighboring region free of GP zones (a result of solute depletion) was also observed, but occurs with a statistically unknown number density because of the small volume examined by TEM.

Coring, or microsegregation of Cu during solidification, had a pronounced effect on GP zone size and distribution. The regions richest in Cu, near the edges of the dendrites, contained a very dense zone structure, with individual zones about 10 nm in diameter (Fig. 2A). Intermediate Cu levels resulted in a somewhat lower density of zones, although the zones were significantly larger (up to 20 nm in diameter) (Fig. 2B). The Cu-poor regions, near the dendrite centers, contained a low density of GP zones, with diameters from 18 to 22 nm. Close inspection of this region revealed a second distribution of GP zones, consisting of a large number of very fine zones, typically 3 nm in diameter (Fig. 2C).

Electron diffraction patterns for the Cu-rich and Cu-poor regions confirm the presence of GP zones. In a cube orientation, Bragg reflections from the fcc matrix planes occur as bright spots in a square array. Reflections from the GP zones appear as continuous streaks because of the very thin disk morphology of the zones (one unit cell in thickness). The continuous nature of the streaks shows that the zones are monoatomic layers of Cu atoms known as GPI zones: streaks from GPII zones, or θ", would show intensity maxima halfway between the fcc Bragg reflections (13). The streaks are very pronounced in regions with dense GP zones (Fig. 2A, inset) and are only barely visible in the regions with small amounts of Cu (Fig. 2C, inset).

The appearance and bimodal distribution of GP zones in the *Flyer* crankcase can be understood in terms of the phase diagram (Fig. 3) that describes the metastable equilibrium between α-Al and GP zones as well as the equilibrium Al-θ(Al₂Cu) system. The requirements for precipitation of a phase (whether stable or metastable) are (i) sufficient supersaturation for nucleation of the precipitate or for spinodal decomposition (a thermodynamic instability whereby nucle-

F. W. Gayle, Metallurgy Division, National Institute of Standards and Technology, Gaithersburg, MD 20899, USA. E-mail: fgayle@nist.gov.
M. Goodway, Conservation Analytical Laboratory, Smithsonian Institution, MRC 534, Washington, DC 20560, USA.

1015